Mechanism and Biological Role of Nitric Oxide Binding to Cytochrome *c*′

Anatoly L. Mayburd*

Department of Molecular Biophysics and Physiology, Rush University, Rush Presbiterian St Luke's Medical Center, Chicago, Illinois 60612

Richard J. Kassner

Department of Chemistry, University of Illinois at Chicago, Chicago, Illinois 60607

Received January 18, 2002; Revised Manuscript Received July 17, 2002

ABSTRACT: The binding of nitric oxide to ferric and ferrous *Chromatium vinosum* cytochrome *c*′ was studied. The extinction coefficients for the ferric and ferrous nitric oxide complexes were measured. A binding model that included both a conformational change and dissociation of the dimer into subunits provided the best fit for the ferric cytochrome *c*′ data. The NO (nitric oxide) binding affinity of the WT ferric form was found to be comparable to the affinities displayed by the ferric myoglobins and hemoglobins. Using an improved fitting model, positive cooperativity was found for the binding of NO to the WT ferric and ferrous forms, while anticooperativity was the case for the Y16F mutant. Structural explanations accounting for the binding are proposed. The NO affinity of ferrous cytochrome *c*′ was found to be much lower than the affinities of myoglobins, hemoglobins, and pentacoordinate heme models. Structural factors accounting for the difference in affinities were analyzed. The NO affinity of ferrous cytochrome *c*′ was found to be in the range typical of receptors and carriers. In addition, cytochrome *c*′ was found to react with cytosolic light-irradiated membranes in the presence of succinate and carbon monoxide. With these results, a biochemical model of cytochrome *c*′ functioning as a nitric oxide carrier was proposed.

Cytochrome *c*′ is a homodimeric hemoprotein of 14 kD molecular mass (per subunit) that is found in many gram-negative species including photosynthetic (*1*), denitrifying (*2*), nitrogen-fixing (*3*), and sulfur-reducing bacteria (*4*). Cytochrome *c*′ has been shown to consist of a four α-helical bundle structure (*5*−*9*) possessing low overall sequence conservation (*10*). Unlike mitochondrial cytochrome *c*, the heme group is attached at the C-terminus. The heme binding sequence is CKXCH. The histidine following the second cysteine is the proximal ligand, while the sixth coordination site is vacant. The heme iron is pentacoordinate in cytochrome *c*′, similar to that of hemoglobin, myoglobin, catalase, cytochrome P450, and other heme proteins for which ligand/substrate binding is the primary function. In contrast, a hexacoordinate structure is observed for purely electron transport hemoproteins, of which cytochrome *c* is one example.

Recent cytochrome *c*′ knock-out mutant experiments with *Rhodobacter capsulatus* (*11*) have suggested that cytochrome *c*′ may play a role in NO binding. Since cytochrome *c*′ has also been identified in pathogenic species such as *Neisseria menigitidis* and *Bordetella pertussis*, this protein may serve to protect the pathogens against attack by NO produced by the immune system. An investigation of this process would be of medical interest. Additionally, the characteristics of cytochrome *c*′ binding to its gas ligand might yield general mechanisms pertaining to gas ligand binding in cells.

Previous studies dealt with the ligand binding behavior and spectra of ferrous cytochrome *c*′. For example, the binding of CO to *C. vinosum* ferrous cytochrome *c*′ has been investigated in detail. The initial model (*12*) has been expanded (*13*) to include noncooperative binding of CO to each of the two monomers followed by dissociation of the homodimer to bound monomers. In addition to CO, NO was one of the first ligands found to bind to cytochrome *c*′. However, UV/VIS spectra of the ferric and ferrous cytochrome *c*′−NO complexes have only recently been reported (*14*). The spectrum of the ferrous NO complex resembles that of pentacoordinate ferric uncomplexed cytochrome *c*′ in the Soret range, both in extinction coefficients and the peak position (396 nm). The pentacoordinate character of the ferrous cytochrome *c*′−NO complex was established earlier by X-ray crystallographic analyses of a NO complex (*2*) and by Raman spectroscopy (*15*). Recently, the pentacoordinate character of a ferrous cytochrome *c*′−NO complex was confirmed, and the proximal localization of the NO ligand binding site was discussed (*16*, *17*). It has been found that the formation of a pentacoordinate guanylate cyclase NO adduct proceeds through the initial formation of a hexacoordinate state (*18*). This is then converted into a pentacoordinate state by complex biexponential kinetics

* Corresponding author. Phone: 312-942-6749. Fax: 312-942-8711. E-mail: amaybu2@yahoo.com.

[1] Abbreviations: A, absorbance; ANSA, 8-anilino-1-naphthylsulfonic acid; AFU, arbitrary fluorescence units; Å, angstrom; BPB, bromophenol blue; BSA, bovine serum albumin; CO, carbon monoxide; [D], cytochrome *c*′ dimer concentration; [D·NO], cytochrome *c*′ dimer−NO complex, with 1 equiv of NO bound; [D(NO)2], cytochrome *c*′ dimer−NO complex, with 2 equiv of NO bound; [H], free heme; $[H]_T$, total heme; [H·NO], nitric oxide heme complex concentration; K_a, K_1, K_2, K_4, corresponding equilibrium constants; K_h, Henry's constant; [M·NO], cytochrome *c*′ monomer and nitric oxide complex; PDB, Protein Data Bank; sGC, soluble guanylate cyclase; *V*, volume; WT, wild-type; *Y*, fraction of NO bound heme sites.

10.1021/bi020058l CCC: $22.00 © 2002 American Chemical Society
Published on Web 09/04/2002

whose fast and slow components were investigated and identified. The same sequence of events seems likely to occur in the case of ferrocytochrome *c*′, which shares spectral similarity with soluble guanylate cyclase (sGC). Similar ligand migration through the packed protein interior between the distal and proximal sites of the heme pocket of myoglobin has been reported (*19*).

To our knowledge, no quantitative studies of NO binding to ferric and ferrous cytochrome *c*′ have been reported that allows for a comparison with available data for other hemoproteins or that yields interpretations of protein structure and function. In this study, the results of spectrophotometric titrations of ferric and ferrous cytochrome *c*′ from *C. vinosum* with NO are described. On the basis of these results, we propose a new binding model involving cooperativity, and a dimer to monomer equilibrium. We also propose a broader biochemical model of cytochrome *c*′ that incorporates its function as a nitric oxide carrier.

MATERIALS AND METHODS

Nitrogen gas was supplied in standard tanks by AGA GAS, Inc., at a purity not less than 99.99%.

Nitric oxide was generated by reaction of sodium nitrite with sodium iodide in the presence of hydrochloric acid according to:

$$2I^- + 2NO_2^- + 4H^+ \rightarrow I_2 + 2NO + 2H_2O \qquad (1)$$

The gas was collected in a eudiometer, and higher oxides of nitrogen were removed by passing the gas through a 1 N NaOH solution.

Recombinant Chromatium vinosum cytochrome c′ was expressed and purified as described earlier (*20*). The concentration of ferric cytochrome *c*′ was determined from the absorption spectrum and the reported extinction coefficient (87 mM^{-1} cm^{-1} per heme) for the Soret band at 399 nm (*21*).

Y16F mutant was prepared using the Transformer Site-Directed Mutagenesis Kit from Clontech (#K1600-1). The plasmid encoding the mutant was extracted from a single colony and the entire gene was sequenced to confirm the presence of the desired mutation (*21*).

Chromatophores (membranes) were isolated anaerobically by using nitrogen-purged buffers and lysis solution throughout the experiment and by maintaining a nitrogen atmosphere above the purged solutions in ultracentrifuge tubes. The *C. vinosum* cell pellet was resuspended at 4 °C in 10 mL/g wet cells solution consisting of 20% sucrose, 50 mM EDTA, and protease inhibitor cocktail (#P8465, Sigma). After 1 h on ice, distilled water containing proteinase inhibitor cocktail was added at 3 mL/g wet cells at 28−30 °C. Cell debris was pelleted at 20 000*g*, and the supernatant was ultracentrifuged at 50 000*g* for 30 min at 4 °C. The membrane pellet was resuspended in 10 mM Tris-HCl (pH 8.0) buffer, and the entire procedure was repeated three times. The washed membrane suspension was stored at 4 °C in the dark under nitrogen.

All spectroscopy was conducted in modified, Thunberg cuvettes with inlet septum adaptors. Cuvettes were purged with N_2, and a stable baseline was established. To initiate a reaction, the sample cuvette was irradiated and/or 10 μL of 1M sodium succinate in Tris-HCl (pH 7.1) buffer was added to the 2.0 mL reaction volume. In the latter case, the imbalance of optical density due to dilution was compensated for by the addition of the same volume of Tris buffer to the reference cuvette.

Spectrophotometric titrations were carried out using a Cary17 UV−vis spectrophotometer. Sample solutions were made anaerobic by exchanging the gas phase above the solution with nitrogen. The ferric cytochrome solution contained 10^{-5} M potassium ferricyanide to maintain the ferric NO complex in the oxidized state. A 100 μL gastight Hamilton syringe was used to deliver aliquots of NO to a solution of the ferric cytochrome *c*′ in the cuvette. To avoid oxidation of NO by atmospheric oxygen, the gas in the syringe needle was exchanged with pure NO by withdrawing and expelling NO gas before the final sampling. After addition of each aliquot of NO, the cuvette was inverted several times and allowed to achieve equilibrium as determined by a constant absorbance value, *A*. Equilibrium was generally observed within approximately 10 min. The partial pressure of NO was determined from the ratio of NO volume added and the volume of the gas phase in the Thunberg cuvette. The liquid-phase concentration of NO was determined from the partial pressure of NO in the gas phase using a Henry's constant of 5×10^4 [L atm/mol] (*22*).

The ratio of NO bound to unbound heme sites was determined by

$$[H{\cdot}NO]/[H] = (A - A_0)/(A_{100} - A) \qquad (2)$$

where [H] is the uncomplexed heme concentration, [H·NO]/[H] the ratio of the concentrations of NO bound to unbound heme sites, *A* the absorbance at each concentration of NO, A_0 the absorbance in the absence of NO, and A_{100} the absorbance at 100% complex.

Several binding models were considered to account for the absorbance changes resulting from the binding of NO to cytochrome *c*′. The simplest binding model assumes that binding of NO to the heme in both subunits is noncooperative and that there is no dimer to monomer equilibrium that affects binding, as follows:

$$H + NO \Leftrightarrow H{\cdot}NO \qquad (3)$$

$$K = [H{\cdot}NO]/[H][NO] \qquad (4)$$

Defining the ratio [H·NO]/[H] as $Y/(1 - Y)$, where *Y* is the fraction of NO bound heme sites and $(1 - Y)$ as the fraction of unbound heme sites gives

$$Y/(1 - Y) = K[NO] \qquad (5)$$

A second binding model assumes that binding of NO to the heme in both subunits is cooperative, where binding of NO to one subunit affects the binding of NO to the second subunit, and that there is no dimer to monomer equilibrium that affects binding, as follows:

$$D + NO \Leftrightarrow D(NO) \qquad (6)$$

$$D(NO) + NO \Leftrightarrow D(NO)_2 \qquad (7)$$

$$K_1 = [D(NO)]/[D][NO] \qquad (8)$$

$$K_2 = [D(NO)_2]/[D(NO)][NO] \qquad (9)$$

The concentrations of NO bound and unbound heme sites

are given by

$$[H{\cdot}NO] = [D(NO)] + 2[D(NO)_2] \quad (10)$$

$$[H] = [D(NO)] + 2[D] \quad (11)$$

Expressing the ratio of NO bound heme sites to unbound heme sites in terms of the unbound dimer concentration gives

$$Y/(1 - Y) = (K_1[NO] + 2K_1K_2[NO]^2)/(2 + K_1[NO]) \quad (12)$$

A third binding model assumes that binding of NO to the heme in both subunits is noncooperative, where successive binding steps occur with equal intrinsic binding constant, K_a, and that there is a dimer to monomer equilibrium of the NO bound dimer that affects the overall binding as follows:

$$D + NO \leftrightarrow D(NO) \quad (13)$$

$$D(NO) + NO \leftrightarrow D(NO)_2 \quad (14)$$

$$D(NO)_2 \leftrightarrow 2M(NO) \quad (15)$$

$$K_1 = [D(NO)]/[D][NO] = 2K_a \quad (16)$$

$$K_2 = [D(NO)_2]/[D(NO)][NO] = K_a/2 \quad (17)$$

$$K_4 = [M(NO)]^2/[D(NO)_2] \quad (18)$$

From the above expressions, the ratio of NO bound to unbound heme sites is given by

$$Y/(1 - Y) = K_a[NO] + \frac{2K_a{K_4}^{0.5}[NO]\,(1 + K_a[NO]\,)}{(K_a{}^2K_4[NO]^2 + 8(1 + K_a[NO])^2[H]_T)^{0.5} - K_a{K_4}^{0.5}[NO]} \quad (19)$$

where $[H]_T$ is the total concentration of heme sites.

A fourth binding model assumes that binding of NO to the heme in both subunits is cooperative and that there is a dimer to monomer equilibrium of the NO bound dimer:

$$D + NO \leftrightarrow D(NO) \quad (20)$$

$$D(NO) + NO \leftrightarrow D(NO)_2 \quad (21)$$

$$D(NO)_2 \leftrightarrow 2M(NO) \quad (22)$$

$$K_1 = [D(NO)]/[D][NO] \quad (23)$$

$$K_2 = [D(NO)_2]/[D(NO)][NO] \quad (24)$$

$$K_4 = [M(NO)]^2/[D(NO)_2] \quad (25)$$

From the above expressions, the ratio of NO bound to unbound heme sites is given by

$$Y/(1 - Y) = \frac{K_1[NO](1 + 2K_2[NO])}{2 + K_1[NO]} + \frac{4(1 + K_1[NO] + K_1K_2[NO]^2)(K_1K_2K_4)^{0.5}[NO]}{(2 + K_1[NO])\{(K_1K_2K_4[NO]^2 + 8[H]_T(1 + K_1[NO] + K_1K_2[NO]^2))^{0.5} - (K_1K_2K_4[NO]^2)^{0.5}\}} \quad (26)$$

The ratios of NO bound to unbound heme sites determined from the absorbance at various concentrations of NO, according to eq 2, were fitted to each of the above models using the Sigmaplot 2000 statistical package (SPSS Incorporated).

Ferrous cytochrome c′−NO complex was prepared in sodium ascorbate. The stock was prepared by rapidly dissolving dry ascorbic acid in nitrogen-purged 0.1 M phosphate buffer and bringing the pH to 7.0. After verification of the pH, the solution was purged with nitrogen once more and kept under a septum to prevent rapid accumulation of oxidation products after exposure to atmospheric oxygen. A 10 μL sample of this 1 M ascorbate stock solution per 2.0 mL of degassed ferric cytochrome *c′* solution was sufficient to cause slow and almost complete reduction. The NO binding constant to ferrous cytochrome *c′* was estimated by the simplest binding model (*5*), using the concentration of NO for half saturation. The concentration of NO in equilibrium with cytochrome *c′* was calculated after subtraction of the amount bound by cytochrome *c′*:

$$[\Delta NO] = RT(V_l/K_hV_g)Y[H]_T \quad (27)$$

$$[NO]_0' = [NO]_0 - [\Delta NO] \quad (28)$$

where $[\Delta NO]$ is the drop in NO liquid-phase concentration due to cytochrome *c′* binding, Y is the faction of NO bound heme, $[H]_T$ is the total heme, V_l and V_g are the volumes of the liquid and the gas phase in the cuvette, respectively, $[NO]_0'$ is the resulting NO liquid-phase concentration after correction, $[NO]_0$ is the uncorrected concentration, and $K_h = 5 \times 10^4$ L atm/mol, Henry's constant for NO in water (*22*).

Hazardous procedures. Liquid-phase concentrations of NO above 2 mM were achieved by creating excess pressure in the quartz Thunberg cuvettes. Cuvettes must be checked for cracks and wrapped in a tissue. Extra pressure under the septum should not exceed 2 atm.

RESULTS

Panels A and B of Figure 1 show the absorption spectra of ferric and ferrous cytochrome *c′* and the ferric and ferrous cytochrome *c′*−NO complexes in the Soret region as well as in the α,β region. Absorption maxima and extinction coefficients of the ferric and ferrous cytochrome *c′*−NO complexes are compared in Table 1 with those for horse heart myoglobin. Figure 1 shows that the absorption spectrum of the WT ferric cytochrome *c′*−NO complex is similar to that observed previously (*2*). As previously noted (*14*), the ferric NO complex is isoelectronic with the ferro CO complex. Consequently, the spectra are very similar and both are characterized by α and β absorption bands in the visible

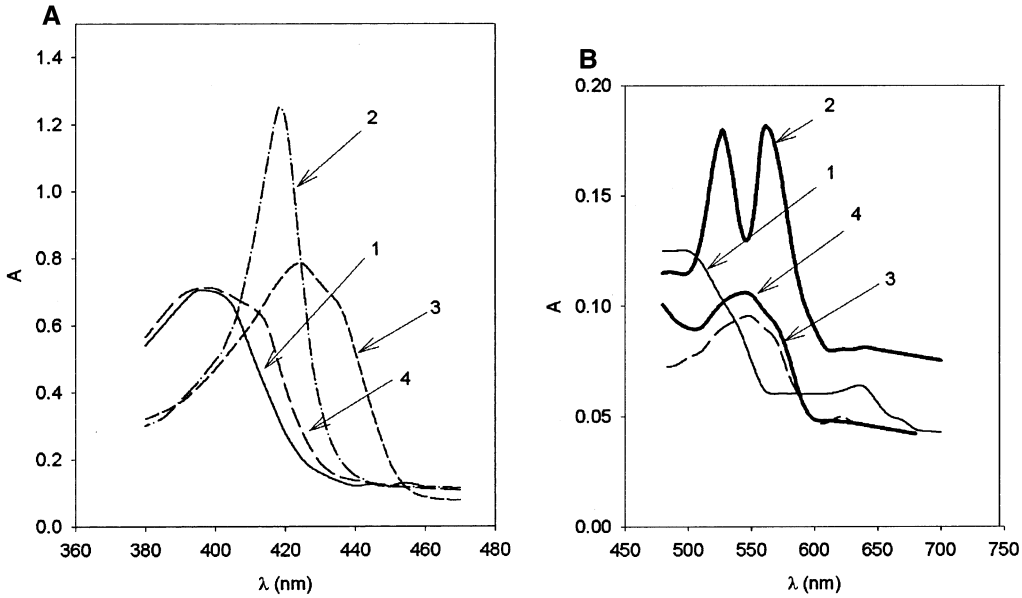

FIGURE 1: (A) Spectra of ligand-free and NO-complexed *C. vinosum* cytochrome *c′* (8μM heme) in the 470−380 nm range. 1, ferric cytochrome *c′*; 2, ferric NO-complexed cytochrome *c′*; 3, ferrous cytochrome *c′*; 4, ferrous NO-complexed cytochrome *c′*. (B) The spectra of ligand-free and NO-complexed *C. vinosum* cytochrome *c′* (8μM heme) in the 700−470 nm range. 1, ferric cytochrome *c′*; 2, ferric NO-complexed cytochrome *c′*; 3, ferrous cytochrome *c′*; 4, ferrous NO-complexed cytochrome *c′*.

Table 1: Absorption Maxima and Extinction Coefficients of NO-Complexed and Uncomplexed Ferric Hemoproteins

	absorption maxima (nm) and extinction coefficients (L mmol^{-1} cm^{-1}) per heme			
protein	region γ		region β	region α
C. vinosum WT cytochrome *c′*				
uncomplexed ferric[a]	400 (87)		495 (10.2)	635 (2.7)
NO-complexed ferric[a]	418 (188)		530 (28.1)	561 (28.1)
uncomplexed ferrous[a]	424 (94)	437sh (87)	541 (14)	
NO-complexed ferrous[a]	397 (88)	414sh (80)	541 (17.1)	
horse heart myoglobin				
uncomplexed ferric[b]	408 (188)		502 (10.2)	630 (3.9)
NO-complexed ferric[c]	420.5 (155)		530 (10.5)	572 (10.3)
uncomplexed ferrous[b]	435 (121)			
NO-complexed ferrous[b]	421.5 (147)			

[a] Data obtained in our experiments. [b] Ref *27*. [c] Ref *26*.

range. The X-ray structure for ferrocytochrome *c′*−CO complex is known (1E86A, PDB), and CO occupies the distal position. A surface hydrophobic patch around the distal heme site that binds BPB dye was described in an earlier work (*20*). Both CO and NO ligands were found to compete with BPB dye for binding to the patch (data not shown), indicating that both approach the same site. Although an X-ray structure for the ferric cytochrome *c′*−NO complex has not been published, the combination of spectral and biochemical evidence suggests that the distal heme site is the most likely position for the NO ligand in the ferric complex. The hexacoordinate intermediate was also observed for the ferrous complex (*18*). One can conclude that formation of a hexacoordinate distal site NO complex is the initial step in NO binding by both ferric and ferrous cytochrome *c′*. Furthermore, the structural factors affecting the formation of this complex must also affect the overall binding constant, even if the hexacoordinate form is transient, as in the case of ferrous cytochrome *c′* binding.

The extinction coefficients of *C. vinosum* cytochrome *c′* and its NO complex presented in Table 1 are somewhat higher than those previously reported for ferric cytochrome *c′*−NO complexes (*14*). It is noteworthy that in the absence of added potassium ferricyanide, some ferro cytochrome *c′*−NO complex was formed from the ferric cytochrome *c′*−NO, presumably due to a much higher affinity of reduced cytochrome *c′* for NO.

Figure 2 shows the results of a spectrophotometric titration of *C. vinosum* ferricytochrome *c′* with nitric oxide at pH 7.0 and 100 mM ionic strength in the presence of 10^{-5} M potassium ferricyanide (to suppress reduction of a high potential NO complex).

Figure 3A shows plots of $Y/(1 - Y)$ versus NO concentration for different concentrations of WT heme. The plots indicate that the extent of complex formation at each ligand concentration is dependent on the heme concentration (Table 2). The extent of complex formation increases as the heme concentration decreases, as previously reported for CN^- (*23*) and CO (*13*) binding to *C. vinosum* ferri and ferrocytochrome *c′*, respectively. The results of the spectrophotometric titration of ferricytochrome *c′* with NO demonstrate the earlier observed pattern. The pattern was explained by dissociation of the ligand-bound dimer to monomers. The existence of a predominantly monomeric state of ferrocytochrome *c′* after CO binding was demonstrated directly by gel-exclusion chromatography using CO-saturated reducing buffer (*21*). The same experiment for NO binding turned out to be more complicated technically due to NO reactivity and instability.

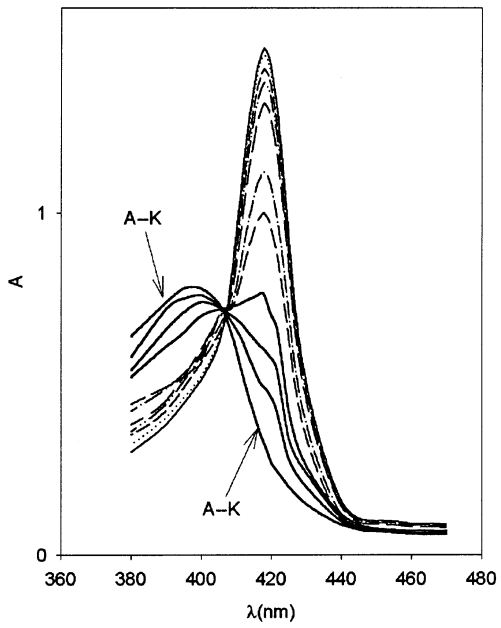

FIGURE 2: Titration of ferricytochrome *c′* by nitric oxide at 8 μM heme. Concentrations (M) of nitric oxide from A to K: 0, 2.66×10^{-5}, 5.4×10^{-5}, 1.35×10^{-4}, 2.9×10^{-4}, 4.5×10^{-4}, 7.3×10^{-4}, 1.01×10^{-3}, 1.54×10^{-3}, 2.5×10^{-3}, and 6×10^{-3}.

Consequently, another approach was applied. If the subunits of the homodimer dissociate, the hydrophobic interface must be exposed. A polarity sensitive fluorescent probe, ANSA, was added to nitrogen-purged cytochrome *c′* (Figure 3B) in the absence of the gas ligands. A big hydrophobic surface patch is known to exist around the distal heme site (*20*). As expected, a blue shift in the emission maximum and an increase in the emission intensity were observed. The magnitude of these changes, however, were lower than those observed by the equivalent amount of BSA, due to energy transfer to the heme group, a very powerful quencher within several Å from the donor. Addition of CO to ferrous or NO to ferric cytochrome *c′* increased the observed fluorescent signal by 25%, indicating the opening of a new hydrophobic surface upon gas ligand binding. No conformational changes exposing the protein hydrophobic interior upon ligand binding are found after examination of CO-complexed cytochrome *c′* X-ray structures, leaving the exposed interface as the only possible source of the signal. The observed increase in fluorescence kinetically followed the UV−vis spectral changes and was concomitant with all the transitions involved. The increase in fluorescence that followed CO addition was abolished after CO was displaced by NO, having a higher affinity to ferrous heme. The fluorescence after NO addition returned to the initial level prior to the addition of CO to ascorbate-reduced cytochrome *c′*. The patterns observed in the experiment strongly suggest that the break up of a hydrophobic interface takes place in the hexacoordinate complexes, both for CO and NO, but does not take place in the pentacoordinate NO complex. We concluded that the ferrous cytochrome *c′*−NO complex is dimeric.

The present model differs from that reported earlier (*13*), which postulated the presence of identical binding constants for both subunits and dispersion of the interface as a result of binding to both subunits. In the present model, binding

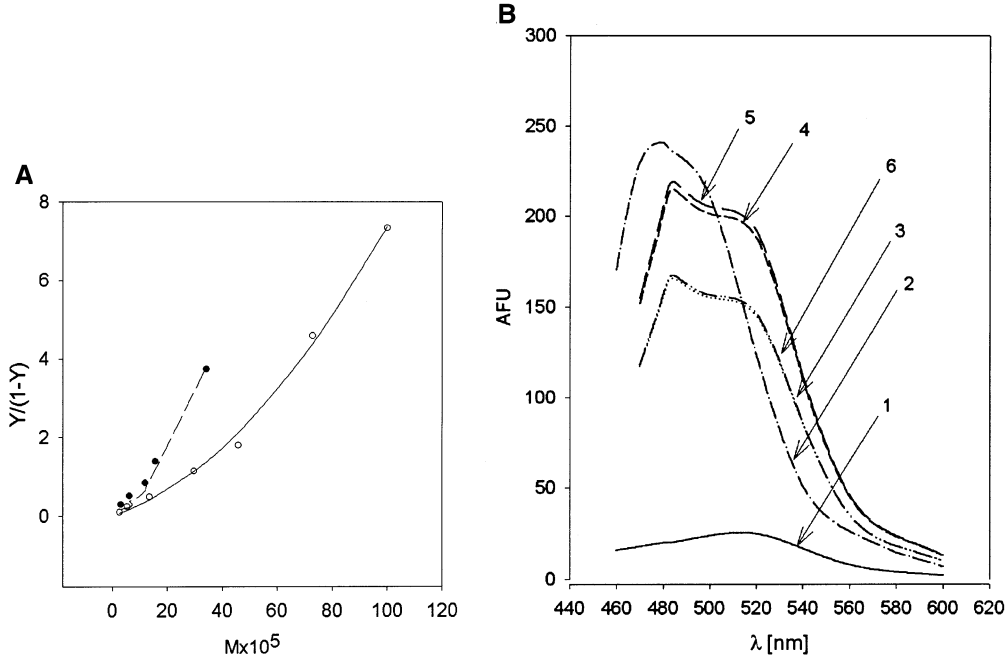

FIGURE 3: (A) Plot of the WT [Bound/Unbound] ferricytochrome *c′* ratio as a function of the NO concentration at two different heme concentrations. Filled circles, experimental data at 1.8 μM heme and 3.12×10^{-5}, 6.25×10^{-5}, 10.56×10^{-5}, 15.6×10^{-5}, and 34.3×10^{-5} M nitric oxide; empty circles, experimental data at 8 μM heme and 2.66×10^{-5}, 5.4×10^{-5}, 1.35×10^{-4}, 2.9×10^{-4}, 4.5×10^{-4}, 7.3×10^{-4}, and 10.10×10^{-4} M nitric oxide. The fitted lines, corresponding to the 20−26 dissociation and cooperativity model, are shown together with the experimental data. Fitted parameters: $K_1 = 3.4 \times 10^2$ [M^{-1}], $K_2 = 3.4 \times 10^3$ [M^{-1}], $K_4 = 5.8 \times 10^{-5}$ [M]. (B) The effect of NO and CO ligand additions upon the hydrophobicity induced ANSA (1.0 μM) fluorescence in the presence of 4 μM cytochrome *c′* (heme). Shown are emissions at 450 nm excitation. 1, ANSA alone; 2, 4 μM BSA added to ANSA, the ordinate scaled down to a 1:5 ratio; 3, cytochrome *c′* added to ANSA, followed by inner filter correction (NO was absent); 4, same as in 3, but NO gas was injected at a 1.5 mM liquid-phase concentration; 5, same as in 4, but NO was absent (cytochrome *c′* was reduced by ascorbate prior to being used and CO was added to 1.6 mM); 6, same as in 5, but NO was added to 1.6 mM and CO to 0.1 mM.

Table 2: Binding Affinities for Ferric Heme Proteins, Determined by Direct Measurement and by Calculation, Using Reported On and Off Rate Constants

protein	k_{on} [M^{-1} s^{-1}]	k_{off} [s^{-1}]	affinity by model *5* [M^{-1}]	affinity by model *26*
Chromatium vinosum ferric WT cytochrome *c′*	–	–	10^4 (at 1.8 μM heme)	$K_1 = 3.4 \times 10^2$ [M^{-1}]
			3×10^3 (at 8 μM heme)	$K_2 = 3.4 \times 10^3$ [M^{-1}] $K_4 = 5.8 \times 10^{-5}$ [M]
Chromatium vinosum ferric Y16F cytochrome *c′*	–	–	2.9×10^5 (at 1.9 μM heme)	$K_1 = 1.1 \times 10^5$ [M^{-1}]
			1.5×10^5 (at 8.4 μM heme)	$K_2 = 1.9 \times 10^4$ [M^{-1}] $K_4 = 1 \times 10^{-4}$ [M]
Mb^+ sperm whale[a]	5.3×10^4	14	3.8×10^3	–
Mb^+ elephant[a]	2.2×10^7	40	5.5×10^5	–
Hb^+ opossum,[a] α chain	3.3×10^3	2.1	1.6×10^3	–
Hb^+, oppossum[a]	1.7×10^3	0.65	2.6×10^3	–
nitrophorine 2 and 3[b]	–	–	5×10^7	–
nitrophorine 1 and 4[b]	–	–	$(1-2) \times 10^6$	–

[a] Ref *28*. [b] Ref *29*.

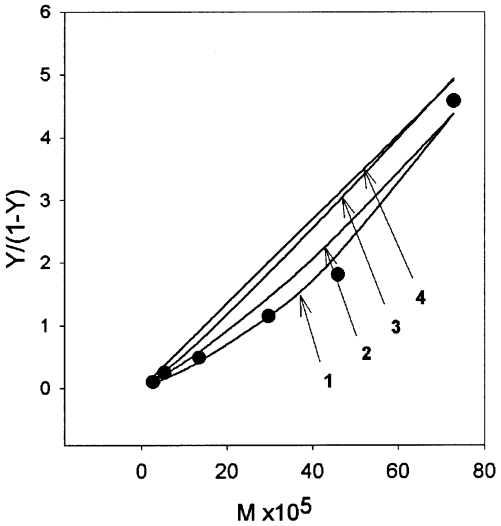

FIGURE 4: Comparison of different fitting models. Filled circles, experimental data. Fitted lines are designated by arrows. 1, dissociation and cooperativity model, fitted parameters $K_1 = 3.4 \times 10^2$ [M^{-1}], $K_2 = 3.4 \times 10^3$ [M^{-1}], and $K_4 = 5.8 \times 10^{-5}$ [M]; 2, cooperativity-only model, fitted parameters $K_a = 1.8 \times 10^3$ [M^{-1}] and $K_4 = 1.5.4 \times 10^{-4}$ [M]; 3, dissociation-only model, fitted parameters $K_1 = 8.7 \times 10^3$ [M^{-1}] and $K_2 = 3.8 \times 10^3$ [M^{-1}]; 4, no dissociation, no cooperativity model, fitted parameters $K = 6.7 \times 10^3$ [M^{-1}].

by the first subunit of the homodimer effects the affinity of the second subunit. After ligand has bound to both subunits, the dimeric state is lost to yield the requisite monomers. Figure 4 compares the fit of the ratio of NO bound to unbound heme sites versus NO concentration for the four different ligand binding models that were compared at the same heme concentration. The results show that the best fit of the data is achieved by employing a model that includes both cooperative binding and dissociation of the dimer to monomer.

The observed binding cooperativity can be rationalized by considering that the binding of a ligand causes movement of the Tyr16 residue. The Tyr16 in 1BBH (PDB) and the residues that occupy the 16th position in the other structures (1E83A, 1CGO, 1CGN, 1JAFA, and 1CPR in PDB) sterically hinder the approach of ligand to the heme iron from the distal side (Figure 5). The 16th residue must be displaced in order for cytochrome *c′* to form a hexacoordinate complex with an incoming ligand. This displacement causes movement of helix A (containing Tyr16) which perturbs the hydrophobic contact between the dimer interface residues, thus affecting both subunits. Figure 5 shows the structural elements participating in the proposed mechanism of cooperative NO binding to ferric cytochrome *c′* and to its Y16F mutant. Tyr16 is stabilized through the formation of a hydrogen bond with Tyr58. If Tyr16 sterically blocks ligand binding, the removal of Tyr16 stabilization by Tyr58 might be expected to significantly affect the binding. Figure 6 presents the results of Y16F mutant titration by NO at different heme concentrations and at fixed ionic strength. The CD spectrum of the Y16F mutant was similar to that of the WT. Compared to the WT UV−vis spectrum, the mutant demonstrated the same extinction coeffcients as those of the ferric, ferrous, and CO-complexed forms. Only a minor red shift of the 437 nm "shoulder" of the ferrocytochrome *c′* spectrum was observed, indicating that the heme environment did not change profoundly by replacing Tyr16 with Phe, a residue of similar size and polarity. At higher temperatures, however, the stability decreased (*24*). A marked concentration dependence of the $(Y/1 - Y)$ function was observed (Figure 6), indicating that, as is the case with WT, complete disruption of the interface takes place in ferric Y16F. As expected, the binding constant, K_1, is 3 orders of magnitude higher than that in the WT, indicating that the Tyr58−Tyr16 hydrogen bond is important for the stabilization of the Tyr16 position and that this hydrogen bond competes with the incoming ligand. The comparison of half-saturation points for WT and Y16F (Figures 3 and 6) shows a 50-fold difference in affinity, corresponding to ~7 kJ/mol per heme contribution in stabilization energy, which can be attributed to the hydrogen bond. The contribution of the interface ($K_a \sim 10^4$) is ~10 kJ/mol heme, as fitting Equation 26 suggests (Table 2). Incoming ligand therefore has to overcome an energy barrier of 15−20 kJ to occupy the distal site.

Figure 7A shows the results of titrating ferrocytochrome *c′* with NO and Figure 7B presents the calculated [bound]/[unbound] as a function of NO. According to the data presented in Table 3, the binding constant of NO to WT ferrocytochrome *c′* is much greater than that of the WT ferric form. Binding proceeded by complex biphasic kinetics,

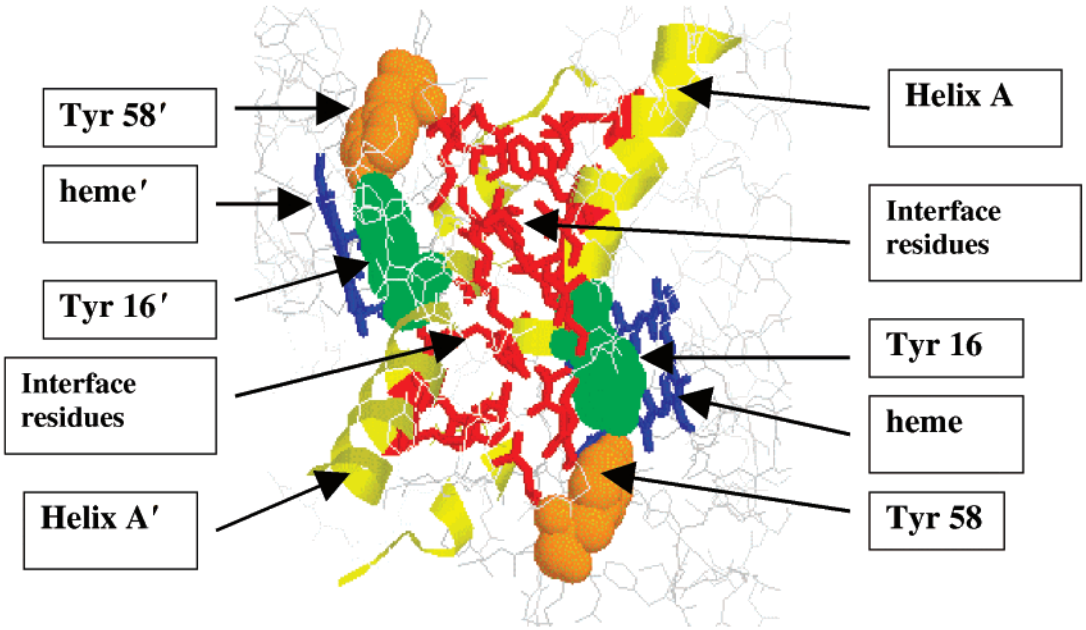

FIGURE 5: Cross section of the interface region between the two subunits of the cytochrome *c*′ homodimer illustrates the proposed mechanism that allows for cytochrome *c*′ cooperative ligand binding. The heme is in blue, Tyr16 is in green, and Tyr58 is in brown for both contacting subunits. The interface amino acid side chains (Ren et al., 1993) are shown in red and belong to helices A (Thr11, Ala14, Glu17, Phe18, Trp21, and Lys25) and B (Ala41, Val45,Ala48, Ile49, Ser52, Gly53, Met54, and Leu57), as well as their identical counterparts in the second subunit (A′, B′).

described earlier for another cytochrome *c*′ (*15*−*17*). The binding of NO was reversible when ascorbate was the reducing agent but irreversible when sulfide was used as reducing agent. Notwithstanding, the NO affinity of the ascorbate-reduced ferrocytochrome *c*′ was found to be much lower compared to the affinities of other pentacoordinate heme systems such as hemoglobin and myoglobin (Table 3). The ANSA fluorescence experiments previously referred to (Figure 3B) suggest dimerization at the stage of the pentacoordinate complex. The data seem to be in agreement with the X-ray structure of NO-complexed ferrous *Alcaligenes xylosoxidans* cytochrome *c*′, where the side chain of position 16 does not deviate from that position occupied in the uncomplexed protein.

Figure 8 describes the redox behavior of cytochrome *c*′. Anaerobically purified and freshly isolated *C. vinosum* chromatophores were added to ferric cytochrome *c*′ in the presence of sodium succinate and CO. After intense illumination using a tungsten lamp, partial reduction of cytochrome *c*′ was observed. Reduction was not observed in the absence of cytochrome *c*′, exogenous succinate, or light (Figure 8). Cytochrome *c*′ in the absence of chromatophores was not reduced by succinate but was reduced by sulfides, hydroquinone, and ascorbate (data not shown). These observations suggest that cytochrome *c*′ may react with members of the succinate dehydrogenase branch of the electron transport chain. The fact that only CO-complexed ferrous cytochrome *c*′ began to form under these conditions indicates a relatively high-potential redox partner and oxidative character of the hypothetical spontaneous reaction in the absence of CO.

DISCUSSION

We found that different intrinsic association constants can describe the binding of NO to the cytochrome *c*′ homodimer

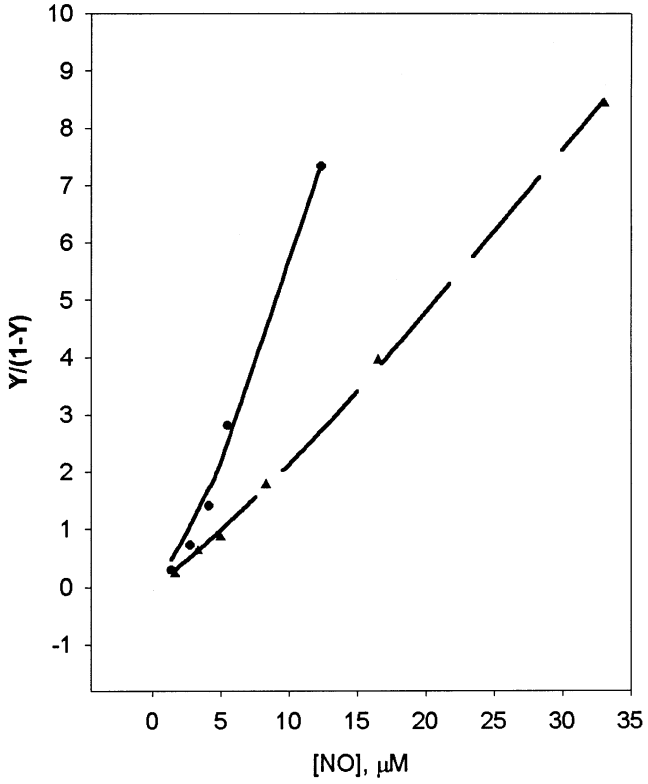

FIGURE 6: Plot of the Y16F mutant [bound/unbound] ferricytochrome *c*′ ratio as a function of NO concentration at two different heme concentrations. Circles, 1.9 μM heme and 1.4×10^{-6}, 2.7×10^{-6}, 4.1×10^{-6}, 5.5×10^{-6}, and 12.3×10^{-6} M nitric oxide. The fitted curve is shown by a solid line. Triangles, 8.5 μM heme and 1.7×10^{-6}, 3.3×10^{-6}, 4.9×10^{-6}, 8.3×10^{-6}, 16.5×10^{-6}, and 33.0×10^{-6} M nitric oxide. The fitted curve is shown by a dashed line, where the parameters used were according to the model 20−26: $K_1 = 1.1 \times 10^5$ [M^{-1}], $K_2 = 1.9 \times 10^4$ [M^{-1}], and $K_4 = 1 \times 10^{-4}$ [M].

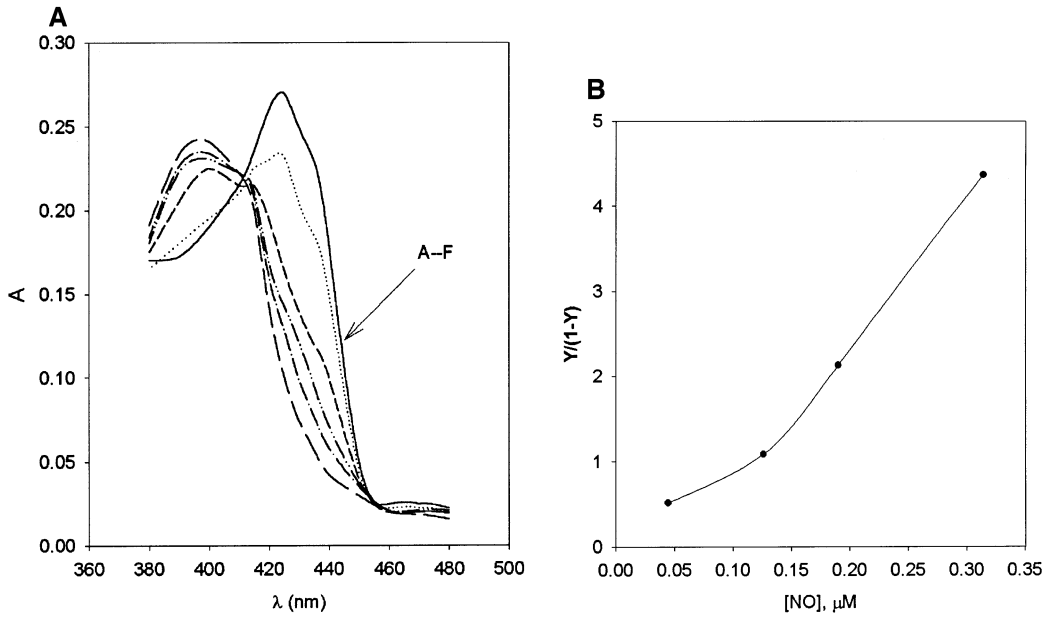

FIGURE 7: (A) Titration of ferrocytochrome *c′* by nitric oxide at 2.8 μM heme. 100 mM phosphate (pH 7.0) and 5×10^{-3} M ascorbate Concentrations (M) of nitric oxide from A to F: 0, 4.45×10^{-8}, 12.6×10^{-8}, 19.0×10^{-8}, 3.14×10^{-7}, and 12.6×10^{-7}. (B) Plot of the [•] ferrocytochrome *c′* ratio as a function of the NO concentration. The $Y/(1 - Y)$ data were collected at 430 nm, using the intermediate data points in shown in Figure 7A.

Table 3: Binding Affinities of NO to Ferrous Proteins and Models, Found by Direct Measurement and by Competition with Carbon Monoxide

protein	affinity $[M^{-1}]$[a]		
	NO	CO	O_2
Chromatium vinosum cytochrome *c′*	8×10^6 (at 2.9 μM heme)	7×10^4 [b]	N/A
horse myoglobinc	3.5×10^{11}	2.1×10^7	5.6×10^5
rabbit hemoglobin	4.2×10^{10}	5.4×10^6	–
heme octapeptide	2.4×10^{12}	9.5×10^8	–
protoheme	8.4×10^{12}	4.0×10^9	1.1×10^7

[a] Binding affinities are presented as association constants, corresponding to the elementary fitting model (*5*), and constants for systems other than cytochrome *c′* were previously determined (26).

and that dissociation of the homodimer into individual subunits takes place in the hexacoordinate state. The NO binding constant of cytochrome *c′*, compared to that of myoglobin and hemoglobin, was equivalent in the ferric state but much lower in the ferrous state. The pentacoordinate ferrous form was found to be dimeric. The previous data and our results suggest that the lower NO affinity of ferrous cytochrome *c′* compared to that of myoglobin is due to the mass effect of the displaced proximal histidine and the disruption of the interface. The rupture of the heme iron–histidine bond is an endothermic process, where the binding of nitric oxide results in a smaller binding constant. This observation is in contrast with the results for hemoglobin and myoglobin, where the heme–histidine bond is intact during NO binding and is broken only when the T state is stabilized (see Perutz mechanism, in ref *25*). It is interesting to note that the affinity of ferrous horse myoglobin for NO is $\sim 4 \times 10^4$ greater than the affinity of NO for WT cytochrome *c′*, while the same ratio for CO binding is only $\sim 3 \times 10^2$ (Table 3). The difference is obviously due to varying strengths of competition in proximal and distal environments. Binding data are presented in Table 4, where the affinities of different carrier proteins and receptors for

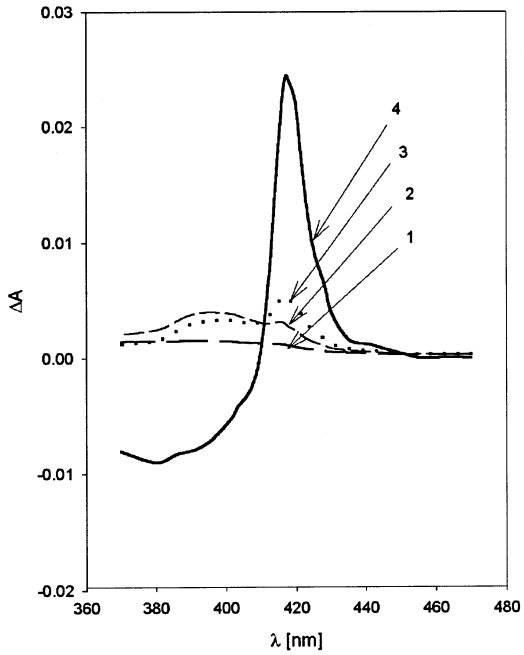

FIGURE 8: Effect of irradiation (15 min at 50 Wt/m^2) and succinate addition (5 mM at pH 7.1) upon the differential absorbance of the chromatophore–cytochrome *c′* mixture under 1 atm of CO partial pressure.The initial chromatophore OD is 1.0 at 372 nm (maximum), and cytochrome *c′* is 2 μM by heme. 1, baseline-corrected differential absorbance signal in the absence of cytochrome *c′* following irradiation and addition of succinate. 2, baseline-corrected differential absorbance signal after addition of cytochrome *c′* with no irradiation and no succinate. 3, same as line 2 after irradiation, but with no succinate. 4, same as line 2 after irradiation and addition of succinate.

their respective ligands are summarized. Since the affinities are in the nanomole to micromole range, fast off rates can occur. If NO binding to ferrous cytochrome *c′* was as strong as it is to hemoglobin/myoglobin (0.01–0.1 nM), then cytochrome *c′* could not turn over rapidly, and would be effectively blocked. The steric and electronic factors that

Table 4: Affinities of Selected Biological Ligands

binding site and function		ligand	affinity (nM)	ref
nitrophorines (NO carriers)				
NP1	pH 5.0	NO	120	*30*
	pH 8.0		850	
NP2	pH 5.0		–	
	pH 8.0		20	
NP4	pH 5.0		50	
	pH 8.0		540	
flavohemoglobin (nitric oxide dioxigenase)		NO	280	
		NADH	4800	*31*
		O_2	10^5	
soluble guanylate cyclase (NO sensor)		NO	250	*21*
synaptosomal receptor		Cl-substituted benzodiazipines	up to 2−5	*32*
calretinin (EF hand containing protein, Ca^{2+} carrier)		Ca^{2+}	500−1500	*33*
chromatium vinosum ferrocytochrome *c′*		NO	120	our results

modulate the affinity are central to the functioning of the protein. The interaction of Tyr16 (and similar side chains in different cytochrome *c′* families) with subunit interfaces might serve to decrease the "on" rate during the initial formation of the hexacoordinate complex. The mass effect of the displaced proximal histidine serves to increase the "off" rate of the final pentacoordinate complex. Comparing the distal and proximal sites within the same cytochrome *c′* system, the mass effect of the displaced Tyr16 side chain and disruption of the interface that accompanies this displacement must be taken into account in estimating the relative stability of the NO ligand in both environments. This factor supposedly contributes to the preferential proximal versus distal ligand localization in the ferrous form. This complements the proximal stabilization of the bound NO by the side chain of Arg124 (*17*), which is conserved (at a position +4 downstream of the heme binding domain, CXXCHXXXR) in all cytochrome *c′* members studied thus far. The hypothetical sequence of events leading to the formation of the final pentacoordinate complex can be summarized as follows:

(1) Competition of NO with the positionally conserved 16th side chain drives the initially distal NO ligand into its proximal location. The ligand and proximal histidine compete for the heme iron, inducing strain on the iron−heme bond but not rupturing it.

(2) The second NO ligand occupies the distal side and binds the heme iron from the distal direction, straining the proximal His−Fe bond even further. Eventually, the His−Fe bond breaks, changing the conformation of the distal pocket.

(3) After the conformational change, increased steric competition between the distal NO and the 16th side chain induces NO to leave the distal pocket. The proximal NO remains "locked" at its site, being stabilized by the Arg at the +4 position. An additional ~15−20 kJ/mol per heme energy barrier must also be overcome, in an effort to displace the 16th side chain and disrupt the interface, if the ligand is to leave the proximal position.

Indeed, the heme plane in CO and NO ferrous complexes of *Alcaligenes xylooxidans* cytochrome *c′* is puckered in different directions, with a stronger distal steric competition for the NO-induced pucker. The proposed mechanism providing binding attenuation and cooperativity in cytochrome *c′* greatly resembles the adjustment of oxygen affinity in hemoglobin. In both cases, the binding energy of a ligand serves to move an α-helix mechanically connected to a hydrophobic interface (*25*). Cytochrome *c′* has been proposed to serve as a simple model of ligand binding behavior as it might relate to medically important sGC (*15*−*17*). In light of our findings, the connection between the two requires examination in more detail. The NO binding constant to the ferrous form is found to be in the range typical of carriers and receptors. This alone would be insufficient to assign a biological role to cytochrome *c′*, but taken in the context of other studies, it becomes significant. In addition to gene knockout experiments (*11*) that demonstrated a connection between the presence of cytochrome *c′* and resistance to NO, our reconstitution experiments using purified *C. vinosum* chromatophores indicated electron transport activity between cytochrome *c′* and membranes (Figure 8). On the basis of the accumulated information, we propose the following model detailing a function of cytochrome *c′* as a nitric oxide protective carrier:

(1) Cytochrome *c′* gets reduced by a low-potential periplasmic redox partner and binds NO with high affinity, protecting most of the periplasmic components against nitrosilation.

(2) The ferrous cytochrome *c′*−NO complex undergoes passive diffusion until contact with the surface of a cytosolic membrane, where the complex gets oxidized by high-potential unidentified membrane partners.

(3) The lower stability of the ferric complex frees the NO ligand near the membrane surface, creating a sufficiently high local NO concentration to diffuse into lipid bilayer to allow for the efficient functioning of NO reductase (1JFB, PDB).

Thus, the combination of a reversible carrier and the NO reductase may clear NO more efficiently than the separate components, while protecting the bulk of the periplasmic components against nitrosilation.

ACKNOWLEDGMENT

We are grateful to Dr. Y. Tan, who conducted mutagenesis of cytochrome *c′* and characterized the mutant. We are also grateful to J. Hui, who helped to express and purify the sufficient amounts of cytochrome *c′*, and to Dr. F. Cohen for critical reading of the manuscript.

REFERENCES

1. Meyer, T. E., and Kamen, M. D. (1982) *Adv. Protein Chem. 35*, 105−212.
2. Iwasaki, H., Yoshimura, T., Suzuki, S., and Shidara, S. (1991) *Biochim. Biophys. Acta 1058*, 79−82.

3. Yoshimura, T., Fujii, S., Kamada, H., Yamaguchi, K., Yamanaka, T., and Imai, S. (1972) *Biochem. Biophys. Res. Commun. 46*, 150−154.
4. Schmidt, T. M., and DiSpirito, A. A. (1990) *Arch. Microbiol. 154*, 453−458.
5. Finzel, B. C., Weber, P. C., Hardman, K. D., and Salemme, F. R. (1985) *J. Mol. Biol. 186* (3), 627−643.
6. Yasui, M., Harada, S., Kai, Y., Kasai, N., Kusunoki, M., and Matsuura, Y. (1992) *J. Biochem. (Tokyo) 1* (3), 317−324.
7. Ren, Z., Meyer, T., and McRee, D. E. (1993) *J. Mol. Biol. 234* (2), 433−445.
8. Tahirov, T. H., Misaki, S., Meyer, T. E., Cusanovich, M. A., Higuchi, Y., and Yasuoka, N. (1996) *Nat. Struct. Biol. 3* (5), 459−464.
9. Benini, S., Rypniewski, W. R., Wilson, K. S., and Ciurli, S. (1998) *Acta Crystallogr., Sect. D: Biol. Crystallogr. 54* (Pt 2), 284−287.
10. Ambler, R. P., Bartsch, R. G., Daniel, M., Kamen, M. D., Mc Lellan, L., Meyer, T. E., and Van Beeumen, J. (1981*) Proc. Natl. Acad. Sci. U.S.A. 78* (11), 6854−6857.
11. Cross, R., Aish, J., Paston, S. J., Poole, R. K., and Moir, J. W. (2000) *J. Bacteriol. 182* (5), 1442−1447.
12. Cusanovich, M. A., and Gibson, Q. H. (1973) *J. Biol. Chem. 248* (3), 822−34.
13. Doyle, M. L., Gill, S. J., and Cusanovich, M. A. (1986) *Biochemistry 25* (9), 2509−16.
14. Yoshimura, T., Fujii, S., Kamada, H., Yamaguchi, K., Suzuki, S., Shidara S., and Takakuwa, S. (1996) *Biochem. Biophys. Res. Commun. 1292*, 39−46.
15. Andrew, C. R., Green, E. L., Lawson, D. M., and Eady, R. R. (2001) *Biochemistry 40* (13), 4115−4122.
16. Lawson, D. M., Stevenson, C. E., Andrew, C. R., and Eady, R. R. (2000) *EMBO J. 19* (21), 5661−5671.
17. Andrew, C. R., George, S. J., Lawson, D. M., and Eady, R. R. (2002) *Biochemistry 41* (7), 2353−2360.
18. Stone, J. R., and Marletta, M. A. (1996) *Biochemistry 35* (4), 1093−1099.
19. Srajer, V. (2001) *Biochemistry 40* (46), 13802−13815.
20. Mayburd, A. L., Tan, Y., and Kassner, R. J. (2000) *Arch. Biochem. Biophys. 378* (1), 40−44.
21. Even, M. T. (1995) in *Molecular cloning, sequencing, expression and site directed mutagenesis of chromatium vinosum cytochrome c*′, Dissertation, University of Illinois at Champagne−Urbana, Champagne−Urana, IL.
22. In *CRC Handbook of Chemistry and Physics, 62-nd edition* (Weast, C., Ed.) CRC Press Incorporated, Boca Paton, FL, 1981−1982.
23. Kassner, R. J., Kykta, M. G., and Cusanovich, M. A. (1985) *Biochim. Biophys. Acta 831* (1), 155−158.
24. Tan, Y. (1999) in *Expression and characterization of wild type and mutant Chromatium vinosum cytochrome c*′, Dissertation, University of Illinois at Champagne−Urbana, Champagne−Urana, IL.
25. Voet, D., and Voet, J. (1995) in *Biochemistry* (Nedah, R., Ed.) pp 231−233, John Wiley and sons, Inc., New York.
26. Romberg (1982) in *Absorption spectra and carbon monoxide/nitric oxide equilibria of model heme complexes and hemoproteins*, Dissertation, University of Illinois at Champagne−Urbana, Champagne−Urana, IL.
27. Antonini, E., and Brunori, M. (1971) *Hemoglobin and Myoglobin in Their Reactions With Ligands*, p 19, North-Holland publishing company, Amsterdam.
28. Sharma, V. S., Traylor, T. G., Gardiner, R., and Mizukami, H. (1987) *Biochemistry 26* (13), 3837−3843.
29. Andersen, J. F., and Montfort, W. R. (2000) *J. Biol. Chem. 275* (39), 30496−30503.
30. Andersen, J. F., Ding, X. D., Balfour, C., Shokhireva, T. K., Champagne, D. E., Walker, F. A., and Montfort, W. R. (2000) *Biochemistry 39* (33),10118−10131.
31. Gardner, A. M., Martin, L. A., Gardner, P. R., Dou, Y., and Olson, J. S. (2000) *J. Biol. Chem. 275* (17),12581−12589.
32. Borea, P. A., and Bonora, A. (1983) *Biochem. Pharmacol. 32* (4), 603−607.
33. Schwaller, B., Durussel, I., Jermann, D., Herrmann, B., and Cox, J. A. (1997) *J. Biol. Chem. 272* (47), 29663−29671.

BI020058L